NANO LETTERS

LETTER

pubs.acs.org/NanoLett

Lithium-Assisted Plastic Deformation of Silicon Electrodes in Lithium-Ion Batteries: A First-Principles Theoretical Study

Kejie Zhao,[†] Wei L. Wang,[†,‡] John Gregoire,[†] Matt Pharr,[†] Zhigang Suo,[†] Joost J. Vlassak,[†] and Efthimios Kaxiras*[,†,‡]

[†]School of Engineering and Applied Sciences and [‡]Department of Physics, Harvard University, Cambridge, Massachusetts 02138, United States

ABSTRACT: Silicon can host a large amount of lithium, making it a promising electrode for high-capacity lithium-ion batteries. Recent experiments indicate that silicon experiences large plastic deformation upon Li absorption, which can significantly decrease the stresses induced by lithiation and thus mitigate fracture failure of electrodes. These issues become especially relevant in nanostructured electrodes with confined geometries. On the basis of first-principles calculations, we present a study of the microscopic deformation mechanism of lithiated silicon at relatively low Li concentration, which captures the onset of plasticity induced by lithiation. We find that lithium insertion leads to breaking of Si−Si bonds and formation of weaker bonds between neighboring Si and Li atoms, which results in a decrease in Young's modulus, a reduction in strength, and a brittle-to-ductile transition with increasing Li concentration. The microscopic mechanism of large plastic deformation is attributed to continuous lithium-assisted breaking and re-forming of Si−Si bonds and the creation of nanopores.

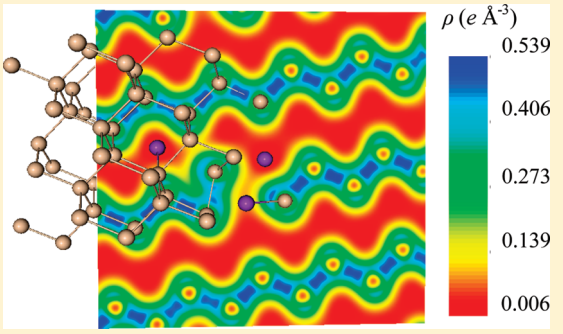

KEYWORDS: Lithium-ion battery, silicon, plasticity, first principles

Energy storage is a crucial aspect of integrating renewable energy sources in power grids, making the development of efficient high-capacity batteries an important technological challenge.[1] For applications that are especially sensitive to weight and size, such as portable electronics and electric vehicles, lithium-ion batteries are the current industry standard.[2] Each electrode in a lithium-ion battery is a host of lithium. During cycles of charge and discharge, lithium diffuses into or out of the electrode, inducing a mechanical deformation and a field of stress in the host frame. In practice, the stress often causes the electrode to fracture or to change its morphology.[3−9] Loss of structural integrity typically reduces the electrical conductance, leading to a steady fading of the capacity during charge−discharge cycles.[10,11]

Mechanical stability is one of the key criteria for the selection of materials for commercial batteries.[12] The electrode material has to maintain its mechanical integrity and chemical properties over a long lifetime. Lithiation-induced fracture not only limits the lifetime of existing commercial batteries but also acts as a bottleneck for developing high-capacity lithium-ion batteries.[13] For example, the extremely high capacity of silicon, which can host up to 4.4 Li atoms per Si atom, has motivated intense research,[14] but the large amount of absorbed Li results in volume swelling of ∼400%, which pulverizes the electrodes. One way to circumvent this mechanical damage is the use of nanostructures, possibly encapsulated by confining oxide layers, which can mitigate the effects of stress by managing the electrode deformation pattern through its shape and geometric restrictions.[15−17]

Recent experiments indicate that the lithiation-induced large deformation of silicon electrodes can be accommodated by plastic flow: during lithiation silicon films deform plastically when the stress exceeds a yield strength.[18] This feature makes it possible to maintain good capacity over many cycles for silicon anodes of small sizes, such as thin films,[19] nanowires,[6] and porous structures.[20] For instance, Takamura et al.[19] have demonstrated fracture-free lithiation of a 50 nm thick silicon film for more than 1000 cycles. During this cycling, the film develops surface undulations, a type of roughening also observed during cyclic lithiation of silicon nanowires.[6] Furthermore, Sethuraman et al.[18] measured lithiation-induced stress as a function of the state of charge in an amorphous silicon thin film and found a pronounced hysteresis, indicating plastic deformation of lithiated silicon. These observations motivated studies of lithium diffusion coupled to the elastic-plastic deformation of the electrode, using continuum plasticity theory.[21−23] While the experimental observations and the modeling of silicon lithiation based on continuum theories provide an understanding of the long-range mechanical properties, the atomic-scale mechanisms that give rise to the plastic behavior remain poorly understood.

We employ first-principles computational methods to explore the atomic-scale mechanisms of lithiation and its relation to mechanical behavior. In particular, we elucidate the microscopic mechanism for the onset of large plastic deformation in lithiated crystalline (c-Si) and amorphous silicon (a-Si), and capture the dramatic brittle-to-ductile transition of a-Si at relatively low lithium concentration. Previous atomistic studies primarily concentrated on elastic properties of the bulk,[24,25] and on

Received: May 5, 2011
Revised: June 15, 2011
Published: June 21, 2011

reproducing the volumetric and electric potential responses during lithiation and delithiation.[26,27] More recently, groups studied the energetics of lithium atoms in bulk crystalline silicon[28] and in silicon nanowires.[29] In this paper, we find that the local atomic structure in a silicon network is altered by lithium insertion, with Si atoms breaking a bond and re-forming a new bond with different neighbors. In this process, the lithiation-induced weakening of bonds between Si atoms and the high mobility of Li in the network play key roles. The continuous breaking and re-forming of Si−Si bonds accommodates the large plastic deformation of lithiated silicon.

The first-principles calculations based on Density Functional Theory (DFT) were performed using the SIESTA code.[30] The crystalline structure is modeled as a 2 × 2 × 2 supercell of the conventional cubic cell that contains eight atoms, with periodic boundary conditions. For consistent comparisons, a supercell containing the same number of Si atoms (64) is employed for the amorphous silicon study. This choice of supercell is consciously relatively small, because we are interested in exploring both a large number of possible configurations (especially for the amorphous case) of Si structures with various Li concentrations and a wide range of perturbations of the equilibrium structures through application of large stresses. Our choice of supercell affords these explorations at a reasonable balance of computational cost and accuracy. The calculated silicon lattice constant is 5.52 Å, slightly larger than the experimental value of 5.43 Å; this difference can be attributed mostly to the generalized gradient approximation for the exchange-correlation functional used in the calculations.[30,31] The atomic structures, system energy, and mechanical stresses are calculated using a local-basis set of double-ζ polarized atomic orbitals with an energy cutoff of 70 Ry (~952 eV). In energy optimization calculations, both the atomic coordinates and the supercell shape were relaxed. The energy optimization was considered complete when the magnitude of the force on each atom was smaller than 0.04 eV Å^{-1}.

As our first topic, we investigate the mechanisms through which the presence of Li atoms in the crystalline silicon lattice can lead to the breaking of Si−Si bonds. We begin this investigation by determining the stable positions of a single lithium atom in c-Si. A single Li atom was placed into the supercell at different nonequivalent sites, shown in Figure 1a, including the tetrahedral site (*Td*), the hexagonal site (*Hx*), the center of a Si−Si bond (*Bc*), the center of the distance between next nearest silicon neighbors (*Cn*), and a substitutional site. In the calculation of the binding energy, we take the energy of an atom in c-Si (E_{Si}) and the energy of an isolated Li atom (E_{Li}) as the reference energies, with $E_{n\mathrm{Li-Si}}$ being the total energy of the system containing n Li atoms in the cell which contains $64 - m$ Si atoms ($m = 0$, except in the case of the substitutional site for the Li impurity, for which $m = 1$). The binding energy per Li atom $E_b(n)$ is

$$E_b(n) = [E_{n\mathrm{Li-Si}} - (64 - m)E_{Si} - nE_{Li}]/n \qquad (1)$$

Table 1 lists the calculated binding energies for lithium in the various positions discussed above; these energies include the basis set superposition error (BSSE) correction. The binding energies at different positions indicate that lithium insertion into the tetrahedral (*Td*) or hexagonal (*Hx*) positions results in an energetically favorable structure. We note that substitution of Si by Li is energetically costly and that the bond center is an unstable position for a Li atom, in contrast to the case of hydrogen atoms in a silicon lattice, for which the most stable configuration is the bond-center site.[32] The binding energy of a single Li at a *Td* position is lower in magnitude than the energy of a Si−Si covalent bond of 2.72 eV,[33] which indicates a relatively weak interaction between the Li and Si atoms. The energy difference of 0.55 eV for a lithium atom at the *Td* and *Hx* sites is close to the diffusion energy barrier reported by Wan et al.,[28] as expected, given the known *Td*−*Hx*−*Td* diffusion pathway for Li in the c-Si lattice. In Table 2, we show the binding energy as a function of the number of Li atoms in c-Si. With increasing occupancy of *Td* sites by Li atoms, the binding energy per Li atom decreases slightly due to the repulsive local interactions between Li atoms. The change in volume upon insertion of Li

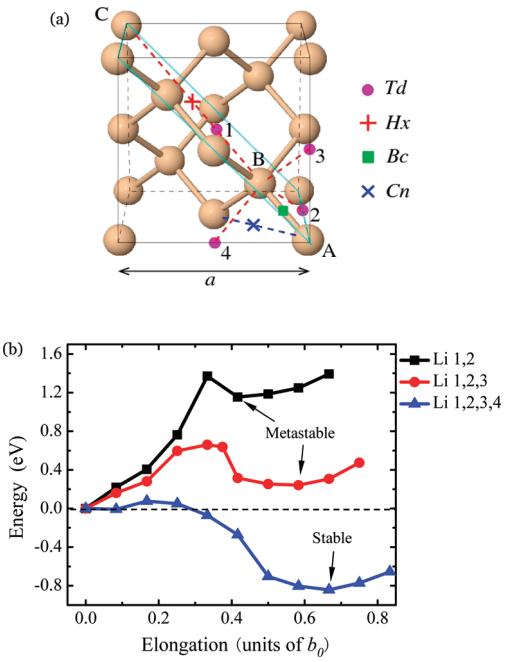

Figure 1. (a) Nonequivalent sites for Li atoms in a c-Si unit cell. The conventional cubic cell of c-Si is outlined by the thin black lines (solid and dashed). The *Td* site is shown as a purple circle, the *Hx* site as a red cross, the *Bc* side as a green square, and the *Cn* site as a blue X (see text for details). Four equivalent *Td* sites (labeled 1, 2, 3, 4), are shown in relation to the pair of Si atoms labeled A and B. The (110) plane outlined in light-blue lines is used for the display of valence charge densities in Figure 2. (b) The total energy as a function of the AB Si−Si bond elongation for different numbers of Li atoms at the *Td* sites around this bond, in units of b_0 = 2.39 Å, the calculated Si−Si equilibrium bond length.

Table 1. The Calculated Binding Energies E_b (in eV) and Relative Volume Changes $\Delta V/V_0$ for One Li Atom at the Various Sites in c-Si Lattice Shown in Figure 1a[a]

Li site	position	E_b (eV)	$\Delta V/V_0$ (%)
substitutional	(0,0,0)	1.37	0.3
center of next nearest neighbors (*Cn*)	($^1/_4$,$^1/_4$,0)	1.39	0.2
bond center (*Bc*)	($^1/_8$,$^1/_8$,$^1/_8$)	1.27	0.8
hexagonal site (*Hx*)	($^5/_8$,$^5/_8$,$^5/_8$)	−0.60	0.4
tetrahedral site (*Td*)	($^1/_2$,$^1/_2$,$^1/_2$)	−1.15	0.2

[a] The Li position is given in Cartesian coordinates and in units of the lattice parameter a of bulk c-Si (the calculated value is a = 5.52 Å).

dx.doi.org/10.1021/nl201501s |*Nano Lett.* 2011, 11, 2962–2967

Table 2. The Calculated Binding Energy $E_b(n)$ and Relative Volume Changes $\Delta V/V_0$ as a Function of n, the Number of Li Atoms in the Crystalline and Amorphous Si Structures at *Td* (in c-Si) and *Td*-like (in a-Si) Positions[a]

	No. of Li (n)	$E_b(n)$ (eV)	$\Delta V/V_0$ (%)
crystalline silicon	1 (f = 0.0156)	−1.15	0.2
	2 (f = 0.0313)	−1.13	0.5
	3 (f = 0.0469)	−1.08	0.9
	4 (f = 0.0625)	−1.03	1.3
amorphous silicon	1 (f = 0.0156)	−1.57	0.4
		[−1.94, −0.55]	[0.2, 0.7]
	8 (f = 0.125)	−1.84	3.3
	16 (f = 0.25)	−1.79	6.4
	32 (f = 0.5)	−1.92	24

[a] Each cell contains 64 Si atoms. f is the concentration of Li atoms in the cell. In the amorphous case, for n = 1, the values represent the average of the 32 lowest-energy *Td*-like positions, while the values in square brackets below the averages show the range from the smallest to the largest value in each case.

atoms in the c-Si lattice is always positive for all the sites considered and is in the range of a fraction of a percent, with the largest change occurring for the *Bc* site.

To demonstrate the atomistic mechanism of lithium-assisted Si−Si bond breaking, we focus on a particular bond. In the simulations, we displace a Si atom B with respect to a fixed Si atom A, imposing a gradual elongation of the AB bond. For each set of fixed positions of A and B, the other atomic positions and supercell shape are relaxed to provide the system energy at the given AB bond length. The displacement of atom B is along a main diagonal of the conventional cubic cell, shown as the red dashed line in Figure 1a, toward the position of the Si atom labeled C. When the bond between atoms A and B is broken, the dangling bonds may be saturated by the neighboring Li atoms. We verify this scenario by examining the energetics of different configurations with two, three, and four Li atoms in the immediate neighborhood of the AB bond. Figure 1b shows the energy profiles as a function of the applied elongation of the AB bond for various Li concentrations (with two, three, and four Li atoms), relative to the system energy when the Li atoms are placed at *Td* positions and no stretch is applied to bond AB. When two or three Li atoms occupy *Td* positions, the initial configurations are the most stable structures, and the energy barriers for transforming to a metastable stretched configuration are 1.37 and 0.66 eV, respectively. However, when four lithium atoms are placed at *Td* sites around the AB bond, the stretched structure is stable and the corresponding energy barrier is only 0.08 eV. Thus, when a single Si−Si bond is surrounded by four Li atoms, the bond readily breaks with a very small energy barrier, and the system reverts to a more stable configuration where one of the Si atoms (B) is displaced to a position close to that occupied originally by the Li atom labeled 1 in Figure 1a.

In order to elucidate the bond breaking mechanism induced by lithiation, we plot in Figure 2a the total valence electron charge density distribution on a (110) plane for the stable configuration with four Li atoms (this plane is highlighted in Figure 1a). Close inspection of this charge density plot shows that the bond between Si atoms A and B is indeed broken, and a weaker bond of mixed covalent−ionic character is formed between the Si atom at position B and the Li atom at position 1.

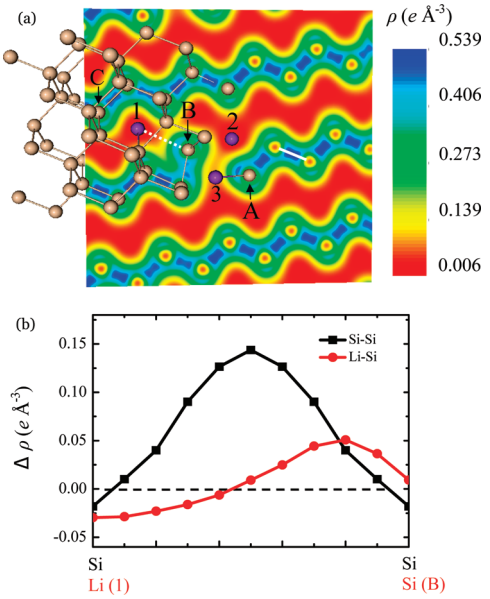

Figure 2. (a) Valence electron charge density distribution on a (110) plane in the lowest-energy configuration of c-Si with four Li atoms. The (110) plane is indicated by light-blue lines in Figure 1a. (b) The charge density difference distribution along a Si−Si bond in pure c-Si represented by a solid white line in (a), and the Li−Si bond 1−B represented by a dashed white line in (a).

This is consistent with the expectation mentioned above that the Li atoms can saturate the dangling bonds of the Si atoms upon bond breaking; the Si−Li bond is expected to be asymmetric and polar, due to the large difference in electronegativity between the two elements (0.98 for Li vs 1.90 for Si).

To better illustrate this point, we show in Figure 2b the charge density difference distribution along a Si−Si bond in the pure silicon lattice and along the Li−Si bond 1−B. The charge density difference $\Delta\rho$ is defined as

$$\Delta\rho = \rho_{n\mathrm{Li-Si}} - \rho_{\mathrm{Si}} - \rho_{\mathrm{Li}} \qquad (2)$$

where $\rho_{n\mathrm{Li-Si}}$, ρ_{Si}, and ρ_{Li} represent the electron densities of the Li−Si system containing n Li atoms in the c-Si supercell, the pure silicon structure consisting of only Si atoms in the same positions as in the Li−Si system, and the contribution from the individual Li atoms at the positions they occupy in the Li−Si system, respectively. The electron density around the Li atom is clearly lower than what it would be near a Si atom in the pure Si crystal, whereas the electron density near the Si atom at position B is higher, indicating a partial electron transfer from the Li atom to the neighboring Si atom. In contrast to the purely covalent bonds in c-Si, which involves a very significant and symmetric electron charge accumulation between a pair of Si nearest neighbors (black symbols and line in Figure 2b), the Si and neighboring Li atoms form a weak bond of mixed ionic−covalent character, with significant charge depletion of the Li atom and charge accumulation closer to the Si atom (red symbols and line in Figure 2b), since the latter is more electronegative.

During operation of a lithium-ion battery, the crystalline silicon electrode is amorphized after the first cycle of charge and discharge.[6] To avoid the stress field induced by this phase transition, amorphous silicon is often used as the electrode in experiments. Intense efforts have been directed toward the

dx.doi.org/10.1021/nl201501s |*Nano Lett.* 2011, 11, 2962–2967

characterization of the plastic deformation behavior of silicon during lithiation and delithiation, both experimentally and theoretically,[18,21−23] but the deformation mechanism responsible for plastic flow has not been elucidated so far. In an attempt to capture the essential atomistic aspects of the plastic deformation mechanisms, we performed a set of simulations that model a uniaxial tension experiment on lithiated silicon at various Li concentrations. The main insight from these simulations is that the plastic deformation is induced by a continuous, lithium-assisted breaking and re-forming of silicon bonds.

The a-Si network is generated by quenching the liquid phase with explicit molecular dynamics using the environment dependent interatomic potential (EDIP) for Si.[34] The resulting amorphous 64-atom supercell is completely free of coordination defects. The details describing this amorphous supercell have been reported elsewhere.[35] We take this cell as representative of the ideal, coordination-defect-free continuous random network that is relevant to the a-Si structure, although the actual amorphous solid is expected to contain defects such as undercoordinated (3-fold) or overcoordinated (5-fold) atoms. The bond-length distribution in this model has a peak at 2.37 Å, close to the calculated bond length in c-Si (2.39 Å), and is quite broad, with values ranging from ∼2.18 to ∼2.65 Å.

We focus here on the equilibrium, static features of lithiated silicon and do not consider kinetic effects, such as long-range diffusion processes of lithium in the silicon structure. We first investigated the stable positions for a single Li atom in the amorphous structure. By analogy to the crystalline case, we considered "*Td*-like" positions for the Li atoms as candidates for the lowest-energy structure. These are positions along the direction of each Si−Si bond, at a distance equal to the Si−Si bond length from each Si atom and away from its nearest Si neighbor. The 64-atom supercell contains 128 Si−Si bonds and therefore there are 256 such *Td*-like positions in the model. To determine the actual lowest-energy positions, we placed a Li atom in each of these *Td*-like positions and then relaxed the whole structure by allowing rearrangement of atomic coordinates as well as relaxation of the supercell shape. Since some of the *Td*-like positions share the same cage of neighboring Si atoms, the relaxation produced 32 unique configurations that are not necessarily a subset of the initial 256 *Td*-like candidates; the Si coordination of the original amorphous structure is maintained in each relaxed structure. We then vary the Li occupancy of these 32 positions to control the concentration f (ratio of the number of Li atoms over the number of Si atoms) in our uniaxial stress simulations. In structures with less than full Li occupancy, such as $f = 0.125$ and $f = 0.25$, the lithium atoms are located at the most energetically favorable sites out of the 32 lowest-energy positions. We note that for all these values of Li concentration the binding energy per Li atom is negative (see Table 2); in other words, it is energetically favorable to insert Li atoms in the amorphous structure, taking as a reference bulk amorphous Si and free Li atoms. Moreover, the values of the binding energy per Li atom in the amorphous case are substantially larger in magnitude than the binding energy per Li atom in the crystalline lattice, suggesting that thermodynamically it is better to insert Li in electrodes consisting of amorphous rather than crystalline Si. Full occupancy of all the *Td*-like sites corresponds to an amorphous structure with $f = 0.50$, well below the theoretical capacity of 4.4 lithium atoms per silicon atom. Nevertheless, even at these relatively low concentrations, we observe pronounced lithium-mediated effects on the mechanical behavior of lithiated silicon. This effect has also been observed in experiments.[18]

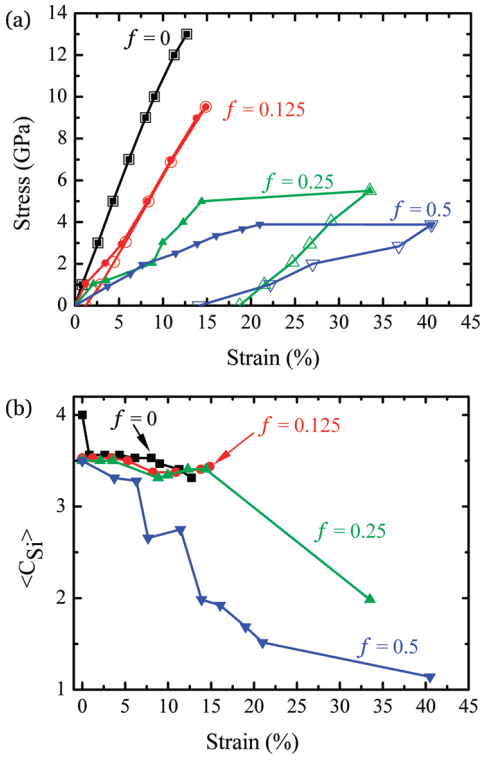

Figure 3. (a) The stress−strain response of lithiated a-Si under uniaxial tension. The solid symbol lines represent the loading path; the open symbol lines represent the unloading path. (b) The average value of Si−Si coordination ($\langle C_{Si} \rangle$) as a function of applied strain during loading.

In the simulation of uniaxial tension, we prescribe a given stress level along the x direction of the structure, and measure the nominal strain after full relaxation. The stress−strain response curves are shown in Figure 3a. For each curve, the highest stress level represents the strength of the lithiated structure before it is fractured. The solid symbol curves represent the loading paths, while the open symbol curves represent the unloading paths. It is evident that a brittle-to-ductile transition occurs as the lithium concentration increases, with very different behavior for $f = 0$ and $f = 0.125$ vs $f = 0.25$ and $f = 0.50$. The corresponding strength decreases as well with increasing Li concentration. In the pure silicon structure, loading leads to nonlinear elastic behavior and the unloading path follows the loading path exactly; there is no permanent deformation after unloading. In the case of lithium concentration $f = 0.125$, a small permanent strain of $\varepsilon = 1.21\%$ is observed after unloading. As the lithium concentration increases to $f = 0.25$ and $f = 0.50$, the stress−strain curves show substantial plastic deformation. The network can be stretched by 33.5% and 40.5%, respectively, without fracture. After unloading, large permanent deformation remains in both cases. Figure 3b shows the average value of Si coordination, $\langle C_{Si} \rangle$, as a function of applied strain. To determine a physically meaningful Si coordination, we define two Si atoms to be bonded if their distance is within 20% of the covalent bond length in bulk c-Si, which corresponds to a largest distance of 2.87 Å. The average coordination is closely related to the deformation behavior of lithiated silicon. At lithium concentrations $f = 0$ and $f = 0.125$, the coordination of silicon changes little during deformation, corresponding to brittle behavior at low Li concentration. In contrast, at larger Li concentration $f = 0.25$ and $f = 0.50$, the Si

dx.doi.org/10.1021/nl201501s |*Nano Lett.* 2011, 11, 2962–2967

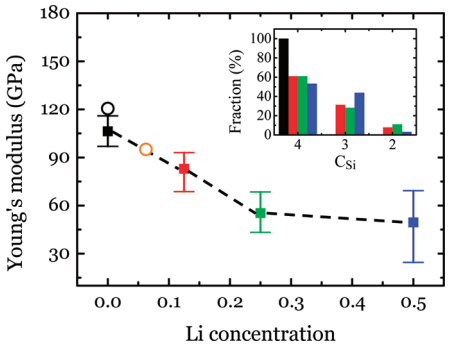

Figure 4. Dependence of the Young's modulus on the concentration of Li. The error bars represent variations due to the anisotropy of the amorphous model structure. The open symbols represent Young's modulus of the pure c-Si lattice (black circle) and of the stable configuration of c-Si with four Li atoms (orange circle). The inset shows the distribution of Si coordination (given as percentage of total number of atoms) in a-Si for different Li concentrations at zero strain. The color of each bar in the inset corresponds to the Li concentration of the same color on the large plot.

coordination decreases dramatically with strain, which is related to the ductile behavior.

Another indication of the very different nature of the mechanical behavior at elevated Li concentrations in a-Si is given by the volume relaxation (see Table 2). The volume relaxation is roughly consistent with the corresponding values in c-Si for concentrations up to f = 0.25 (about 0.4% for n = 1 and proportionally larger for n = 8 and 16) but is considerably higher for f = 0.5, when the volume increase is twice as large as would have been expected from the proportional relation up to f = 0.25. This is indicative of large changes in the structure, which includes formation of nanopores that can easily accommodate the presence of several Li atoms and will respond differently than the uniform solid to external stress, consistent with recent experimental observations on Si nanowires.[36]

Figure 4 shows the dependence of Young's modulus on Li concentration. The solid squares represent the average values of the elastic stiffness constants along the x, y, and z directions and the error bars the effect of the anisotropy of the amorphous structure due to the finite size of the model and the nonuniform distribution of Li atoms on the scale of the supercell. The open circles represent Young's modulus of pure c-Si (black symbol) and of the stable configuration of c-Si with four Li atoms (orange symbol). Evidently, Young's modulus decreases with increasing Li concentration. The inset in Figure 4 shows the Si coordination for different Li concentrations at zero strain. The softening effect induced by lithiation is correlated with an increase of coordination defects at higher Li concentrations, as evidenced by the increasing fraction of 3-fold coordinated Si atoms; this finding is consistent with experimental measurements[37] and other ab initio calculations.[24]

The large plastic deformation observed in our simulations can be traced to the lithium-assisted breaking and re-forming of Si−Si bonds. To illustrate this process, we show in Figure 5 four snapshots along the loading path for the case of lithium concentration f = 0.50. The snapshots show the atom positions at various loading strains. Two Si atom pairs, labeled D, E and F, G, are shown enlarged for better contrast. The snapshots clearly show the evolution of bonding between these two silicon pairs: silicon atoms D−E experience bonding/nonbonding/bonding changes from the initial state to the final state, while silicon atoms

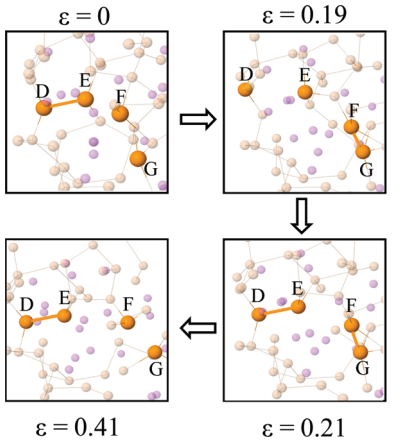

Figure 5. The Si−Si bond breaking and re-forming process during deformation of lithiated silicon at Li concentration f = 0.50. The four snapshots correspond to the states of various strain values ε, as indicated. The two Si atom pairs D−E and F−G that undergo bonding/nonbonding/bonding and nonbonding/bonding/nonbonding transitions are enlarged for better contrast.

F−G undergo nonbonding/bonding/nonbonding changes during the same deformation.

In conclusion, we have studied the effects of Li in both crystalline and amorphous Si, using first-principles calculations based on Density Functional Theory. Our main findings are as follows: first, *Td* interstitial positions are the lowest-energy sites for Li insertion into c-Si, and that when four Li atoms surround a single Si−Si bond the covalent bond readily breaks and the two Si dangling bonds are essentially saturated by the formation of weak bonds of mixed ionic−covalent character with the nearby Li atoms. Also, in a-Si with sufficiently high Li concentration (roughly f = 0.125 or higher) the structure undergoes a brittle-to-ductile transition with significantly lower Young's modulus, and plastic deformation becomes relatively easy. The essence of these results is that the chemical interactions of lithiation give rise to pronounced effects on the mechanical behavior of silicon structures. In particular, as the stresses induced by lithiation are limited by the yield strength, the fracture failure of the silicon electrode can be largely remediated by taking advantage of the plasticity of lithiated silicon. At the microscopic scale, we have identified and described by specific examples the atomistic mechanism responsible for plastic deformation, which consists of continuous Si−Si bond breaking and reformation in the presence of Li. The plastic deformation of solid-like amorphous network in the vicinity of the glass transition point has been attributed to the thermally activated shear transformations around free volume regions,[38] which bears some similarity to the atomic-scale deformations we have described for lithiated a-Si. In the present work we have demonstrated that lithium-assisted bond breaking and re-forming is the mechanism responsible for plastic flow in amorphous silicon at low temperature under strain.

AUTHOR INFORMATION

Corresponding Author

*E-mail: kaxiras@physics.harvard.edu.

ACKNOWLEDGMENT

This work is supported by the National Science Foundation through a grant on Lithium-Ion Batteries (CMMI-1031161) and

by the US Department of Energy through a grant on Hierarchical Petascale Simulation Framework for Stress Corrosion Cracking (DE-FC02-06 ER25790). K.Z. acknowledges helpful discussions with Lauren Hartle. M.P. acknowledges support from the Department of Defense (DoD) through the National Defense Science & Engineering Graduate Fellowship (NDSEG) Program.

REFERENCES

(1) Whittingham, M. S. *MRS Bull.* **2008**, *33* (4), 411–419.
(2) Armand, M.; Tarascon, J. M. *Nature* **2008**, *451* (7179), 652–657.
(3) Huggins, R. A.; Nix, W. D. *Ionics* **2000**, *6* (1−2), 57–63.
(4) Aifantis, K. E.; Hackney, S. A.; Dempsey, J. P. *J. Power Sources* **2007**, *165* (2), 874–879.
(5) Beaulieu, L. Y.; Eberman, K. W.; Turner, R. L.; Krause, L. J.; Dahn, J. R. *Electrochem. Solid-State Lett.* **2001**, *4* (9), A137–A140.
(6) Chan, C. K.; Peng, H. L.; Liu, G.; McIlwrath, K.; Zhang, X. F.; Huggins, R. A.; Cui, Y. *Nat. Nanotechnol.* **2008**, *3* (1), 31–35.
(7) Huang, J. Y.; Zhong, L.; Wang, C. M.; Sullivan, J. P.; Xu, W.; Zhang, L. Q.; Mao, S. X.; Hudak, N. S.; Liu, X. H.; Subramanian, A.; Fan, H. Y.; Qi, L. A.; Kushima, A.; Li, J. *Science* **2010**, *330* (6010), 1515–1520.
(8) Hu, Y. H.; Zhao, X. H.; Suo, Z. G. *J. Mater. Res.* **2010**, *25* (6), 1007–1010.
(9) Zhao, K. J.; Pharr, M.; Vlassak, J. J.; Suo, Z. G. *J. Appl. Phys.* **2010**, *108* (7), 073517.
(10) Arora, P.; White, R. E.; Doyle, M. *J. Electrochem. Soc.* **1998**, *145* (10), 3647–3667.
(11) Wang, D. Y.; Wu, X. D.; Wang, Z. X.; Chen, L. Q. *J. Power Sources* **2005**, *140* (1), 125–128.
(12) Winter, M.; Brodd, R. *J. Chem. Rev.* **2004**, *104* (10), 4245–4269.
(13) Zhang, W. J. *J. Power Sources* **2011**, *196* (1), 13–24.
(14) Kasavajjula, U.; Wang, C. S.; Appleby, A. *J. Power Sources* **2007**, *163* (2), 1003–1039.
(15) Park, M. H.; Kim, M. G.; Joo, J.; Kim, K.; Kim, J.; Ahn, S.; Cui, Y.; Cho, J. *Nano Lett.* **2009**, *9* (11), 3844–3847.
(16) Krishnan, R.; Lu, T. M.; Koratkar, N. *Nano Lett.* **2011**, *11* (2), 377–384.
(17) Song, T.; Xia, J. L.; Lee, J. H.; Lee, D. H.; Kwon, M. S.; Choi, J. M.; Wu, J.; Doo, S. K.; Chang, H.; Il Park, W.; Zang, D. S.; Kim, H.; Huang, Y. G.; Hwang, K. C.; Rogers, J. A.; Paik, U. *Nano Lett.* **2010**, *10* (5), 1710–1716.
(18) Sethuraman, V. A.; Chon, M. J.; Shimshak, M.; Srinivasan, V.; Guduru, P. R. *J. Power Sources* **2010**, *195* (15), 5062–5066.
(19) Takamura, T.; Ohara, S.; Uehara, M.; Suzuki, J.; Sekine, K. *J. Power Sources* **2004**, *129* (1), 96–100.
(20) Kim, H.; Han, B.; Choo, J.; Cho, J. *Angew. Chem., Int. Ed.* **2008**, *47* (52), 10151–10154.
(21) Zhao, K. J.; Pharr, M.; Vlassak, J. J.; Suo, Z. G. *J. Appl. Phys.* **2011**, *109* (1), 016110.
(22) Zhao, K. J.; Pharr, M.; Cai, S. Q.; Vlassak, J. J.; Suo, Z. G. *J. Am. Ceram. Soc.* DOI: 10.1111/j.1551-2916.2011.04432.x.
(23) Bower, A. F.; Guduru, P. R.; Sethuraman, V. A. *J. Mech. Phys. Solids* **2011**, *59*, 804−828.
(24) Shenoy, V. B.; Johari, P.; Qi, Y. *J. Power Sources* **2010**, *195* (19), 6825–6830.
(25) Deshpande, R.; Qi, Y.; Cheng, Y. T. *J. Electrochem. Soc.* **2010**, *157* (8), A967–A971.
(26) Huang, S.; Zhu, T. *J. Power Sources* **2011**, *196*, 3664−3668.
(27) Chevrier, V. L.; Dahn, J. R. *J. Electrochem. Soc.* **2009**, *156* (6), A454–A458.
(28) Wan, W. H.; Zhang, Q. F.; Cui, Y.; Wang, E. G. *J. Phys.: Condens. Matter* **2010**, *22* (41), 415501.
(29) Zhang, Q. F.; Zhang, W. X.; Wan, W. H.; Cui, Y.; Wang, E. G. *Nano Lett.* **2010**, *10* (9), 3243–3249.
(30) Soler, J. M.; Artacho, E.; Gale, J. D.; Garcia, A.; Junquera, J.; Ordejon, P.; Sanchez-Portal, D. J. *J. Phys.: Condens. Matter* **2002**, *14* (11), 2745–2779. We use the PBE exchange-correlation functional, norm-conserving pseudopotentials, and reciprocal-space mesh cutoff equivalent to a 20 Å (10 Å) real-space period for the crystalline (amorphous) supercell..
(31) Juan, Y. M.; Kaxiras, E.; Gordon, R. G. *Phys. Rev. B* **1995**, *51* (15), 9521–9525.
(32) Tuttle, B.; Adams, J. B. *Phys. Rev. B* **1998**, *57* (20), 12859–12868.
(33) Farid, B.; Godby, R. W. *Phys. Rev. B* **1991**, *43* (17), 14248–14250.
(34) Bazant, M. Z.; Kaxiras, E.; Justo, J. F. *Phys. Rev. B* **1997**, *56* (14), 8542–8552.
(35) Mo, Y.; Bazant, M. Z.; Kaxiras, E. *Phys. Rev. B* **2004**, *70* (20), 205210.
(36) Choi, J. W.; McDonough, J.; Jeong, S.; Yoo, J. S.; Chan, C. K.; Cui, Y. *Nano Lett.* **2010**, *10* (4), 1409–1413.
(37) Sethuraman, V. A.; Chon, M. J.; Shimshak, M.; Van Winkle, N.; Guduru, P. R. *Electrochem. Commun.* **2010**, *12* (11), 1614–1617.
(38) Argon, A. S. *Acta Metall.* **1979**, *27* (1), 47–58.